

A Model of Scale Formation on Inner Carbon Steel Pipe Walls for Transporting Hot Spring Water*

Motoaki Morita¹ and Osamu Umezawa²

¹Faculty of Marine Technology, Tokyo University of Marine Science and Technology, Tokyo 135–8533, Japan

²Faculty of Engineering, Yokohama National University, Yokohama 240–8501, Japan

The microstructures of scales adhered to the inner walls of elbow steel pipes, used in the transport of hot spring water, are analyzed. The system examined in this study is from a geothermal plant in Obama town, Unzen city, Nagasaki, Japan, using pipes with 3.5 months of prior use. The adhered substance consists of four layers: amorphous magnesium silicate, aragonite, amorphous magnesium silicate, and iron corrosion products, on the carbon steel from the inside of the pipe to the outside. The corrosion product fully covers the steel surface. The magnesium silicate (1–2 mm thick) is initially generated as an adhesion substance on the corrosion product. The layer thickness of aragonite (orthorhombic calcium carbonate (1-CaCO_3)) is 15–70 nm. Carbon, oxygen and calcium are dissolved in the magnesium silicate, which later precipitates as calcium carbonate with large and/or stratiform features. The chemical contents in the magnesium silicate layers on both the top and bottom sides are nearly identical. Therefore, the precipitation of aragonite and its growth in the magnesium silicate may form the aragonite layer, which shows a columnar structure along the heat flux direction. [doi:10.2320/matertrans.M2016105]

(Received March 25, 2016; Accepted June 6, 2016; Published August 25, 2016)

Keywords: scale adhesion, calcium carbonate, silica, magnesium silicate, geothermal plant

1. Introduction

Geothermal energy, which makes 24-hour power generation possible, is expected to find use in future base load power plants. As such, construction of large-scale geothermal power plants and the industrialization of small-scale geothermal power plants that utilize surplus hot spring water are areas of focus in this field. However, stable operation of such facilities is difficult, and they have not yet seen widespread implementation. One of the major factors inhibiting their stable operation is the adhesion of scales that causes pipe blockage and hinders heat exchange. Therefore, a great deal of recent research in the field has focused on methods of scale suppression and removal for the safe operation of geothermal plants¹. There are two commonly used methods to achieve these aims: pH adjustment through the addition of chemicals to geothermal hot water, and mechanical removal using drills and pressurized water jets. The pH adjustment method is superior to the mechanical removal method in terms of labor and cost, and thus is widely used in geothermal power plants. However, in recent years, there is a demand for scale countermeasures that are more environmentally benign.

Treatment and modification of the material surface of the pipes and heat exchanger can suppress scale adhesion without causing environmental harm. It has been reported that different metals undergo different amounts of scale adhesion^{1–4}, and that this process is also dependent on surface roughness^{1,2}. However, there has been sparse research regarding microstructural control with the end goal of scale suppression in mind. This is due to the lack of crystal metallurgical knowledge of scales adhered in actual geothermal hot water environments. In this study, therefore, we conducted a microstructural analysis of scales adhered to pipes transporting hot water at the Obama hot spring binary power plant in Unzen

city, Nagasaki, and determined the basic structure of scales that adhered in this setting. From the saturation index, we verified the precipitation potential of an adhered scale phase that constitutes the basic structure. In addition, we modeled the formation process of these adhered scales through a layered structure of adhered scales, observation of temporal changes, and microstructural analyses.

2. Experimental Procedure

2.1 Samples

The test material was a JIS G 3452 SGP elbow pipe that was used for the operation of the Obama hot spring binary power plant in Obama town, Unzen city, Nagasaki, from April 1 to July 17 in 2013. Figure 1 depicts the system configuration of areas near where the elbow pipe was installed, indicating the sampling location. Geothermal hot water yielded from the Obama Marina source was passed through the transportation pipe, collected in a hot water storage tank, and transported to a heat exchanger. The distance from the source to the hot water tank was approximately 40 m. The chemical composition of the geothermal hot water in the Obama Marina source is shown in Table 1. The temperature of the hot water that passed through the hot water transportation pipe was 102°C, and its pH was 8.09. There was little change to the

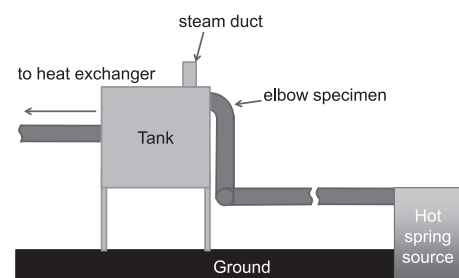


Fig. 1 Schematic diagram of hot spring water transport system set up the elbow pipe near the storage tank of Obama marina hot spring source.

*This Paper was Originally Published in Japanese in J. Japan Inst. Met. Mater. **80** (2016) 309–316. The title and abstract were replaced with more appropriate expression.

Table 1 The chemical contents of hot spring water at both Obama marina and Orange bay hot spring sources.

	Obama marina	Orange bay
Temperature, T/K	375	375
pH	8.09	8.29
Electric conductivity (mS/m)	1352	1363
Total soluble matter (ppm)	9060	9100
Na ⁺ (ppm)	2610	2670
K ⁺ (ppm)	271	300
Ca ²⁺ (ppm)	156	146
Mg ²⁺ (ppm)	160	141
Cl ⁻ (ppm)	4590	4620
SO ₄ ²⁻ (ppm)	358	323
HCO ₃ ⁻ (ppm)	192	162
F ⁻ (ppm)	0.45	0.51
B ³⁺ (ppm)	15.9	17.3
As ⁵⁺ (ppm)	0.269	0.423
Total-SiO ₂ (ppm)	235	270
Stable hydrogen isotope ratio, δD/%	-3.5	-3.6
Stable oxygen isotope ratio, δ ¹⁸ O/%	-0.41	-0.40

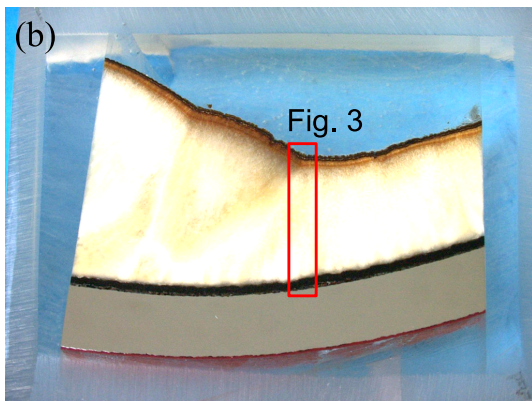
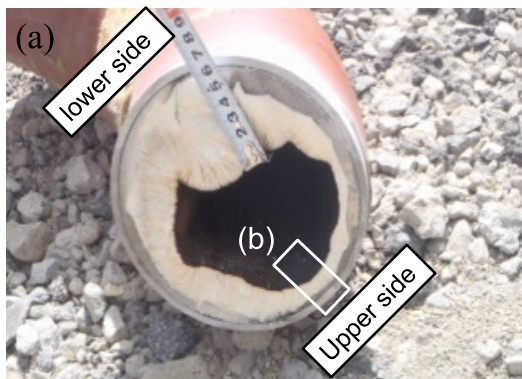


Fig. 2 Elbow pipe specimen in the cross section (a) and the sample taken from the upper side of elbow pipe (b).

composition of the hot spring before and after the installation; however, there was no heat insulation for the pipes with insulation materials.

Figure 2 shows the outer appearance of the test sample at the time of sampling. The test sample consisted of a carbon steel pipe with scales. An appropriate amount of test sample

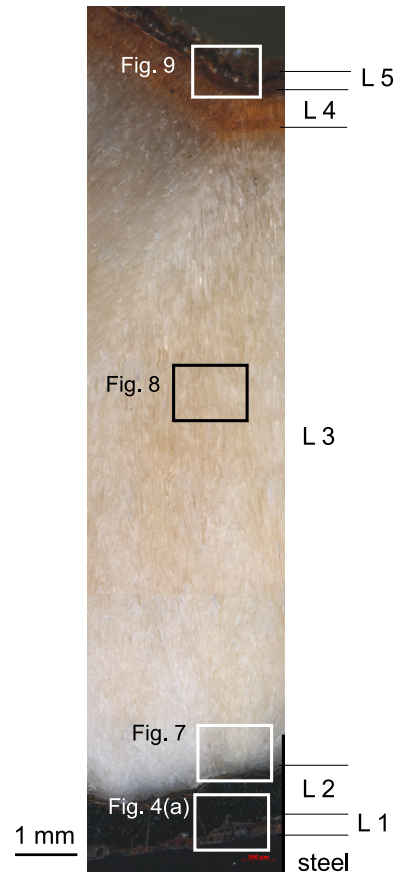


Fig. 3 Optical micrograph of the scale on the carbon steel pipe shown in Fig. 2. The adhesion substance consists of 5 layers, i.e. L1 to L5.

was collected from the upper part of the vertical and horizontal elbow, and was placed in a resin. After polishing the sample with emery paper and alumina suspension, the sample surface was mirror polished (Fig. 2(b)). The outer wall of the pipe was painted with an anti-rust agent.

2.2 Microstructural analyses of scales

Optical microscopy and FE-SEM (field-emission scanning electron microscopy) with an EDS (energy-dispersive spectroscopy) detector were used to characterize the microstructure of the adhered scales. We also used micro X-ray diffraction (XRD) for their phase identification.

2.3 Observation of temporal changes in scales

To observe temporal changes in the thickness of the adhered scales, we installed a JIS G 3452 SGP pipe (outer diameter: 100 A) in the Orange Bay source, 200 m from the Obama Marina source. The temperature, pH, and chemical composition of the Orange Bay source are shown in Table 1. The composition of this hot spring water is similar to that of the water from the Obama Marina source. The water level of the geothermal hot water flowing in the pipe was approximately up to the center of the pipe. The installation period was two months; photographs of the inside of the test piece were taken once a month, and the thickness of the scales was measured based on this information.

3. Experimental Results

3.1 Layered structure of pipe scales and their phase identification

Figure 3 shows a magnified version of the image shown in Fig. 2(b). The scales comprise multiple layers, which are denoted by different colors from the inner wall of the pipe: a mixed layer of black and red, a black layer, a cream-colored layer, a yellow-brown layer, and a black layer. These five layers are labeled L1 to L5, respectively, and their microstructures were characterized.

3.1.1 The L1 layer

The L1 layer has a black to reddish-brown color, and adheres to the whole inner wall of the pipe. Figure 4(a) shows a backscattered electron (BSE) image of the region that extends from the carbon steel to the L1 and L2 layers in Fig. 3. The arrows in Fig. 4(a) mark the embedded resin, indicating that there were gaps present at the time of embedding. Gaps also exist between the L1 layer and the L2 layer. There are similar uneven shapes both above and below these gaps, indicating that the L1 and L2 layers were originally connected. These gaps are assumed to be cracks created by the shear stress that formed at the L1/L2 layer interface due to drying or cooling of the scale during sampling. Our discussion in this paper is based partially on the idea that these gaps were originally connected at the time of scale formation.

The inner region of the L1 layer consists of two types of scales (Fig. 4(b)). The gray part adhering to the carbon steel

surface is labeled as the L1-1 layer, while the black part is labeled as the L1-2 layer. The L1-1 layer is present on the inner wall of the pipe, and its thickness is 20 μm at most. On the other hand, the L1-2 layer has many gaps and a thickness of 10–150 μm . Figure 5 shows the results of compositional analysis conducted at points A to K as shown in Figs. 4(b), 7(b), 8(a), and 9(a). The L1-1 layer (analysis point B) is comprised primarily of Fe and O, while the L1-2 layer (analysis point C) consists of Si, Mg, and O. XRD analysis results for the L1-1 and L1-2 layers are shown in Fig. 6. A diffraction peak for Fe_2O_3 and a broad peak identified as amorphous iron hydroxide are both present at around 30–40° (Fig. 6(a)). The L1-2 layer is amorphous (Fig. 6(b)), and identified as primarily amorphous silica-silicate.

Based on these results, the L1 layer is a two-layer structure consisting of corrosion products of iron (Fe_2O_3 and iron hydroxide) and an amorphous silica-silicate layer that covers these products.

3.1.2 The L2 layer

The thickness of the black L2 layer is 0.7–1.5 mm, and it adheres to the pipe covering the whole surface of the L1 layer (Fig. 2). The main components of this layer (analysis point D) are Si, Mg, and O, and minute amounts of Fe, Ca, and C are

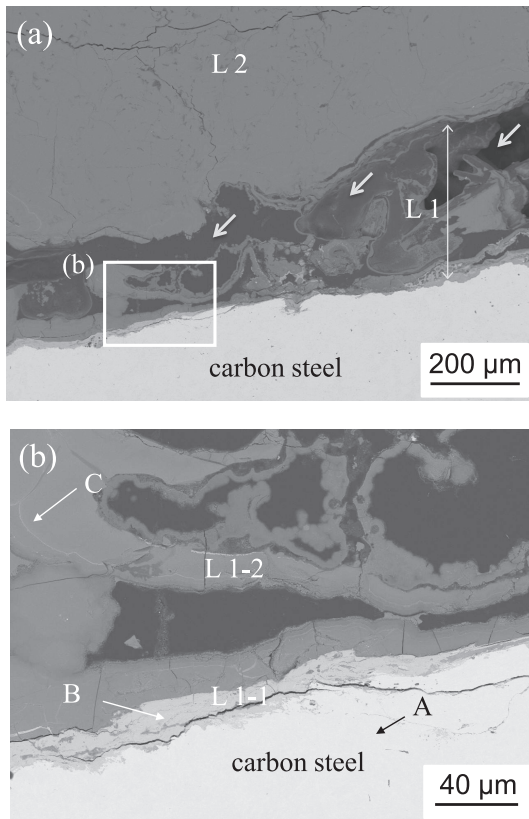


Fig. 4 Backscattered electron image at L1 and L2 layers (a) shown in Fig. 3 and magnified image of L1 layer (b). Arrows in (a) show resin parts. The L1 layer is divided into two parts as L1-1 and L1-2. Analysis points of A to C are indicated in (b).

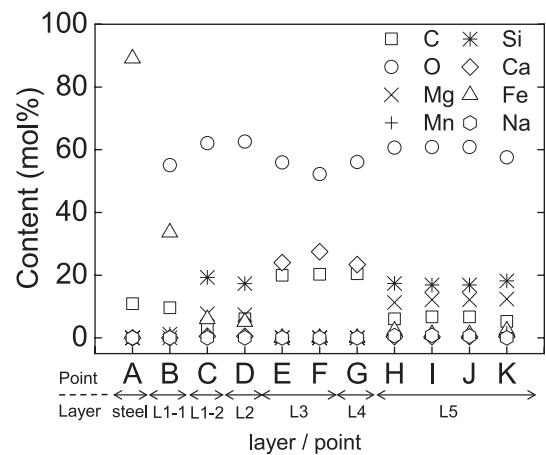


Fig. 5 Chemical contents in each layer with EDS analysis points of A to K.

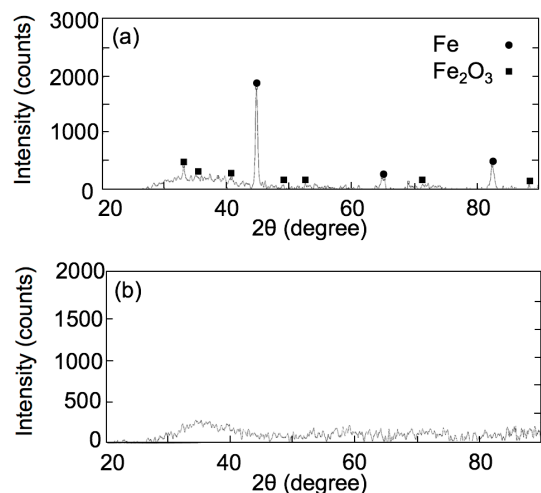


Fig. 6 X-ray diffraction profiles at (a) L1-1 and (b) L1-2 layers.

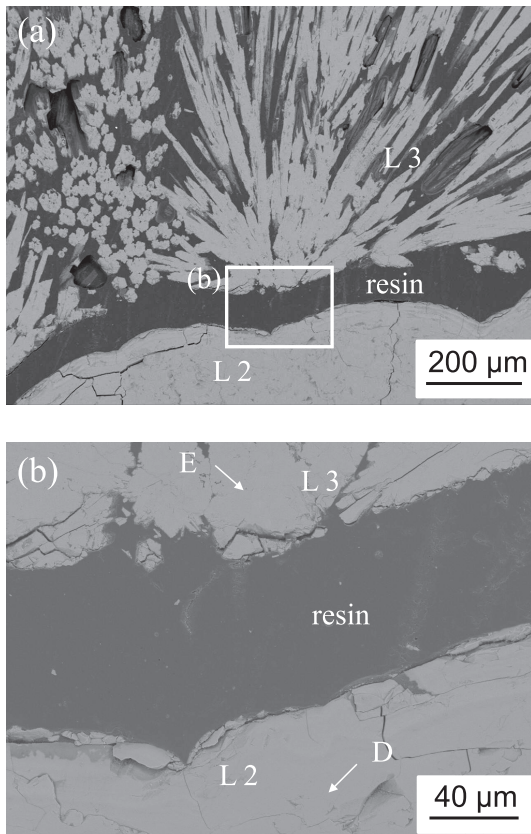


Fig. 7 Backscattered electron image at L2 and L3 layers (a) shown in Fig. 3 and magnified image of their interface (b). Analysis points of D and E are indicated in (b).

also present (Fig. 5). As in the L1-2 layer, this layer is amorphous without exhibiting any clear XRD diffraction peaks, and thus the L2 layer is considered to be amorphous silica-silicate.

The chemical compositions of the L1-2 and L2 layers are almost identical (Fig. 5), and thus the L1-2 and L2 layers are assumed to have originally been the same layer. The L1-2 layer is porous, but pores were not detected in the L2 layer. It is assumed that the amorphous silica-silicate in the L2 layer became denser as it grew.

3.1.3 The L3 and L4 layers

Resin is mixed in between the L2 and L3 layers (Fig. 7). The concavo-convex shapes above and below the L2/L3 interface are similar, and thus the L2/L3 interface is assumed to have originally been connected. The L3 layer is composed of a cream-colored substance (Fig. 3), and the thickness of the L3 layer varies between the inner and outer bends of the elbow pipe. The thickness is 15 mm for the outer bend (upper side) and 70 mm for the inner bend (lower side) (Fig. 2(a)). This result indicates that the velocity of the fluid on the inside surface of the elbow pipe affects the growth rate of the scales. Figure 8 shows a BSE image and XRD pattern of the central part of the L3 layer (Fig. 3). The L3 layer comprises a porous material with columnar crystals, and the dark areas in these images indicate the resin. The main components of the L3 layer (analysis point F) are Ca, C, and O (Fig. 5), consistent with diffraction peaks of the calcium carbonate polymorph, aragonite (orthorhombic crystal) (Fig. 8(b)). In addition, elemental segregation is not detected at the base (analysis point

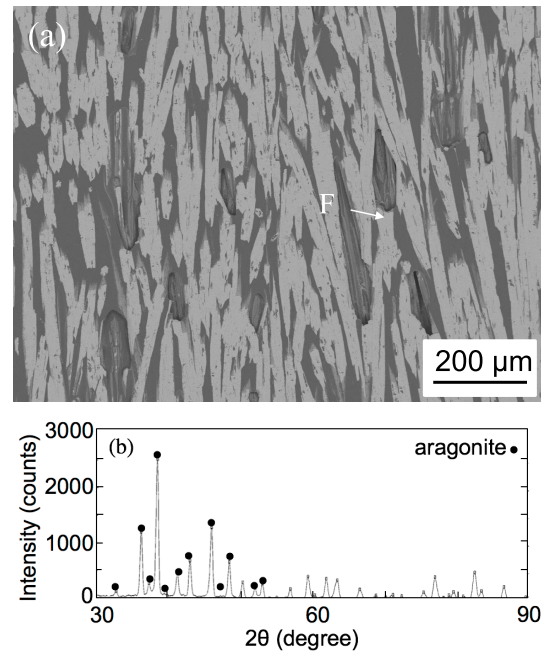


Fig. 8 Backscattered electron image (a) and X-ray diffraction profile (b) in L3 layer shown in Fig. 3. Analysis point of F is indicated in (a).

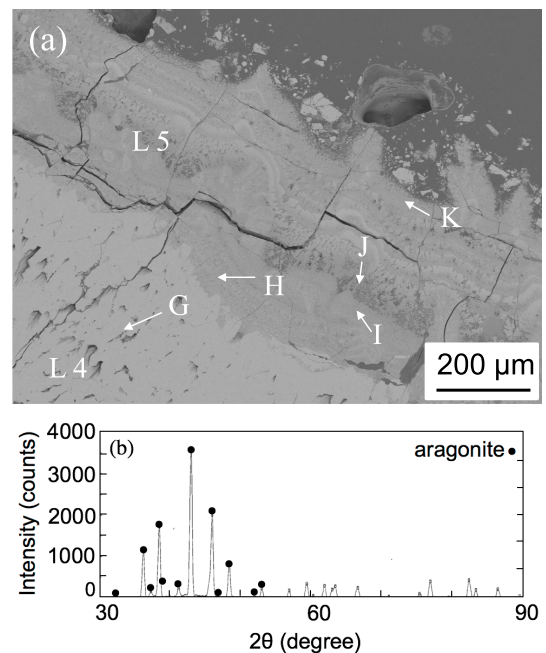


Fig. 9 Backscattered electron image (a) at L4 and L5 layers shown in Fig. 3 and X-ray diffraction profile in L4 layer (b). Analysis points of G to K are indicated in (a).

E) and central region (analysis part F) of the columnar crystal in the L3 layer. The L3 layer consists of porous and columnar aragonite, and does not contain impurities other than the main components of calcium carbonate.

The L4 layer is yellow-brown with a thickness of about 1 mm (Fig. 3). The main components of the L4 layer (analysis point G) are Ca, C and O (Fig. 5), and its XRD peaks are consistent with aragonite (Fig. 9(b)). In addition, the composition of the L4 layer is almost identical to that of the L3

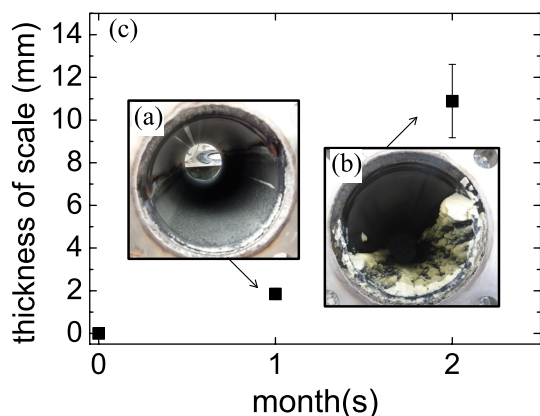


Fig. 10 Scale on the steel pipe after flushing through hot spring water at Orange Bay source: outlooks for 1 month (a) and 2 months (b), and their average thickness of scale (c).

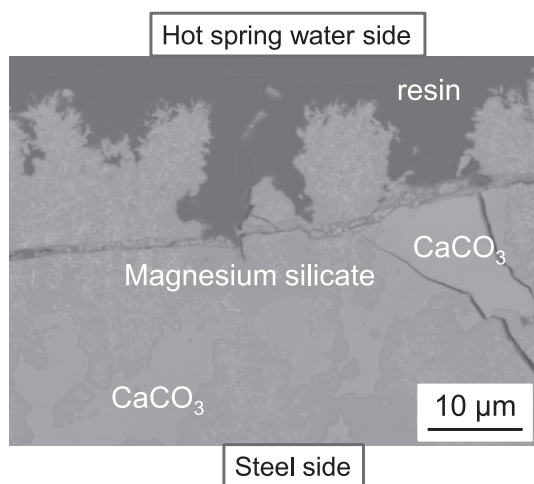


Fig. 11 Backscattered electron image of the cross section at the white color scale surface shown in Fig. 10(b).

layer, and elemental segregation does not appear to be present. The L4 layer has fewer gaps compared to the L3 layer (Fig. 9(a)).

Based on the above results, the L3 and L4 layers are determined to be aragonite layers.

3.1.4 The L5 layer

The L5 layer comprises the black scales on the surface in contact with the flowing hot water (Fig. 3), and its thickness is 0.5–1.0 mm (Fig. 9(a)). The main constituents of the L5 layer are Si, Mg, and O (Fig. 5), and the crystal structure of the layer is amorphous. Therefore, the L5 layer is labeled as amorphous silica-silicate. Within the L5 layer, there is a contrast in the BSE image, with analysis points H, I, J, and K having different contrasts in Fig. 9(b). However, the results of EDS analysis do not show a significant difference in terms of the main components. The Fe concentration is lower than that of the L1-2 and L2 layers. Based on these results, the L5 layer is identified to be single-phase amorphous silica-silicate with Fe impurities.

3.2 Temporal changes in the scale thickness

Figure 10 shows time variation of the scale adherence in

the sample from the Orange Bay source. In the first one month, black scales of thickness ≤ 2 mm are formed (Fig. 10(a)). In the subsequent one month, white scales with a mean thickness of 10 mm are found to adhere on top of these black scales (Fig. 10(b)). The main components of the black scales are Si, Mg, and O, while those of the white scales are Ca, C, and O. Based on these results, the black and white scales are determined to be amorphous silica-silicate and calcium carbonate, respectively. The growth rate of calcium carbonate is five to six times higher than that of amorphous silica-silicate (Fig. 10(c)).

Both white and black scales (amorphous silica-silicate) are observed on the surface of scales formed over two months (Fig. 10(b)). Microstructure analysis of the white scale shows a thin amorphous silica-silicate layer covering the calcium carbonate layer (Fig. 11). Therefore, areas of calcium carbonate that come into direct contact with the geothermal hot water are not observed. This is similar to the layered scale structure found in the pipes of the Obama Marina source.

4. Discussion

4.1 Saturation index of each oxide

Among the substances adhered to the surface of the carbon steel pipe, scales formed by geothermal hot water are comprised of aragonite and amorphous silica-silicate. Therefore, using chemical equilibrium calculations and our experimental results, the dissolution and precipitation of calcium carbonate and silica-silicate in geothermal hot water at the Obama Marina source were evaluated.

First, the dissolution and precipitation reaction of calcium carbonate can be expressed with eq. (1):



Assuming that the acid dissociation equilibrium of carbonate is established, the concentration of carbonate ions is obtained from the 2nd acid dissociation equilibrium, as expressed in eq. (2):



The solubility product and the 2nd acid dissociation constant of the crystalline polymorph of calcium carbonate at 102°C were derived using the temperature function (eqs. (3)–(6)) obtained by Plummer *et al.*⁵⁾

$$\log K_{\text{calcite}} = -171.9065 - 0.077993T + 2839.319/T + 71.595 \log T \quad (3)$$

$$\log K_{\text{aragonite}} = -171.9773 - 0.077993T + 2903.293/T + 71.595 \log T \quad (4)$$

$$\log K_{\text{vaterite}} = -171.1295 - 0.077993T + 3074.688/T + 71.595 \log T \quad (5)$$

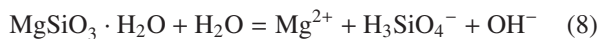
$$\log K_2 = -107.8871 - 0.03252849T + 5151.79/T + 38.92561 \log T - 563713.9/T^2 \quad (6)$$

where K is the solubility product for each polymorph of calcium carbonate. The saturation index (SI) can be defined using eq. (7):

$$SI = \log_{10}(Q/K) \quad (7)$$

where Q is the activity product of each ion present in the geothermal hot water associated with the targeted dissolution and precipitation reactions, and K is the solubility product. Substances under a condition of $SI > 0$ are supersaturated in geothermal hot water, and are unsaturated at $SI < 0$. The values of SI_{calcite} , $SI_{\text{aragonite}}$, and SI_{vaterite} in the geothermal hot water in the Obama Marina source are 2.31, 2.21, and 0.91, respectively, and the crystalline polymorph of calcium carbonate was supersaturated in the geothermal hot water.

There are many types of amorphous silica-silicate: silicon dioxide consisting of SiO_2 only, magnesium silicate consisting of SiO_2 and MgO , and aluminum silicate consisting of SiO_2 and Al_2O_3 . Silicon dioxide dissolves at approximately 450 ppm in pure water at 373 K⁶⁾. The total silica in the geothermal hot water of the Obama Marina source was 245 ppm, and as such silicon dioxide was unsaturated. On the other hand, as shown in Fig. 5, the main elements that constitute precipitated amorphous silica are Si, O, and Mg. Therefore, the dissolution and precipitation reaction of magnesium silicates (MgSiO_3 and $\text{Mg}_3\text{Si}_2\text{O}_5(\text{OH})_4$) merit consideration, as shown in eqs. (8) and (9):



In these reactions, the solubility products K_{MgSiO_3} ⁷⁾ and $K_{\text{Mg}_3\text{Si}_2\text{O}_5(\text{OH})_4}$ ⁸⁾ are obtained using eqs. (10) and (11), respectively:

$$\log(K_{\text{MgSiO}_3}) = -12.90 + 0.00262 \times (T - 273) - 6.212 \times 10^{-5} \times (T - 273)^2 \quad (10)$$

$$\log(K_{\text{Mg}_3\text{Si}_2\text{O}_5(\text{OH})_4}) = 9303/T + 3.283 \quad (11)$$

If we assume that all the silica in hot spring water is ionic silica associated with the dissolution and precipitation reaction, the saturation indices SI at 375 K are $SI_{\text{MgSiO}_3} = 2.79$ and $SI_{\text{Mg}_3\text{Si}_2\text{O}_5(\text{OH})_4} = 9.11$. In other words, magnesium silicate is supersaturated.

The above results demonstrate that supersaturated aragonite and magnesium silicate precipitate and adhere to the carbon steel pipe. However, supersaturated calcite and vaterite were not observed. Based on this information, a scale formation mechanism can be put forth, as discussed in the next section.

4.2 Formation mechanism of the magnesium silicate layer

If we consider the adherence of oxide on a solid surface as nucleation, the nucleation mechanism can be divided between the surface reaction and deposition of particles^{9,10)}. Nucleation via a surface reaction is the bonding (through a chemical reaction) between ionic silica within a solution and a metal surface. Adherence due to deposition occurs as silica particles that formed in solution remain on the inner wall of the pipe due to effects such as gravity. In the case of silica adhesion through a surface reaction, iron oxide and iron hydroxide tend to form the nucleation sites used by silica⁹⁻¹¹⁾. In addition, Hayakawa *et al.*¹²⁾ showed that condensation is one of

the mechanisms by which ionic silica in solution adheres to a glass surface. Iron corrosion products such as Fe_2O_3 and iron hydroxide are present on the pipes analyzed in this study, forming magnesium silicate on top. Nucleation of magnesium silicate in this environment is assumed to be due to a condensation reaction of iron hydroxide (a corrosion product of the carbon steel surface) and supersaturated magnesium silicate.

4.3 Formation mechanism of the calcium carbonate (aragonite) layer

Elemental segregation was not observed in the aragonite layers L3 (analysis points E and F) and L4 (analysis point J) (Fig. 5). In the analyzed pipe, the calcium carbonate layer was always covered by the magnesium silicate layer, and as such the calcium carbonate does not come in direct contact with the geothermal hot water. The calcium carbonate layer is assumed to have nucleated and experienced crystalline growth within the magnesium silicate layer, separating the magnesium silicate layer. Therefore, we will continue the discussion with the assumption that the L1-2, L2, and L5 layers were originally one layer.

As discussed previously, the concentrations of the main elements of magnesium silicate are consistent in the L1-2 layer (analysis point C), the L2 layer (analysis point D), and the L5 layer (analysis points H, I, J, and K). In addition, the concentration of Fe affected by the carbon steel surface decreases from the wall of the pipe towards the side that is in contact with the water flow. This supports the notion that the magnesium silicate layers were originally one layer. Let us now consider the direction of the crystalline growth of precipitated calcium carbonate in the magnesium silicate layer. The direction of crystalline growth of calcium carbonate was disturbed near the L2 layer (Fig. 7(a)), but as it grew, the direction of crystal growth moved to become parallel to the heat flux direction (Fig. 8(a)). This microstructure formation is similar to columnar crystals seen in typical dendrite growth. For example, in the formation of columnar crystals in metal mold casting, crystal nucleation occurs on the chill layer, and crystals grow in the direction opposite to the heat flux¹³⁾. As a result, a columnar crystal structure forms.

The components of calcium carbonate were detected within the adhered magnesium silicate layer (Fig. 5). Figure 12 shows the elemental distribution in the magnesium silicate layer (L1 and L2 layers) in a longitudinal section vertical to the cross section shown in Fig. 3. These components (Ca, C, and O) are widely and uniformly distributed within the magnesium silicate, forming a solid solution. In addition, massive or layered precipitates, with Ca, C, and O as the primary components, are confirmed to be present in the magnesium silicate layer. Ca, C, and O, supplied to the magnesium silicate layer from the geothermal hot water, were present in a solid solution state to begin with, and precipitated as masses or layers of calcium carbonate in the magnesium silicate layer. In order for calcium carbonate to nucleate and grow crystals within magnesium silicate, Ca, C, and O must be continuously supplied from the geothermal hot water via magnesium silicate. One possible mechanism of Ca supply is the diffusion of Ca, C, and O in magnesium silicate. For the diffusion coefficient of Ca in Mg-Si-O, the diffusion constant D_0 and

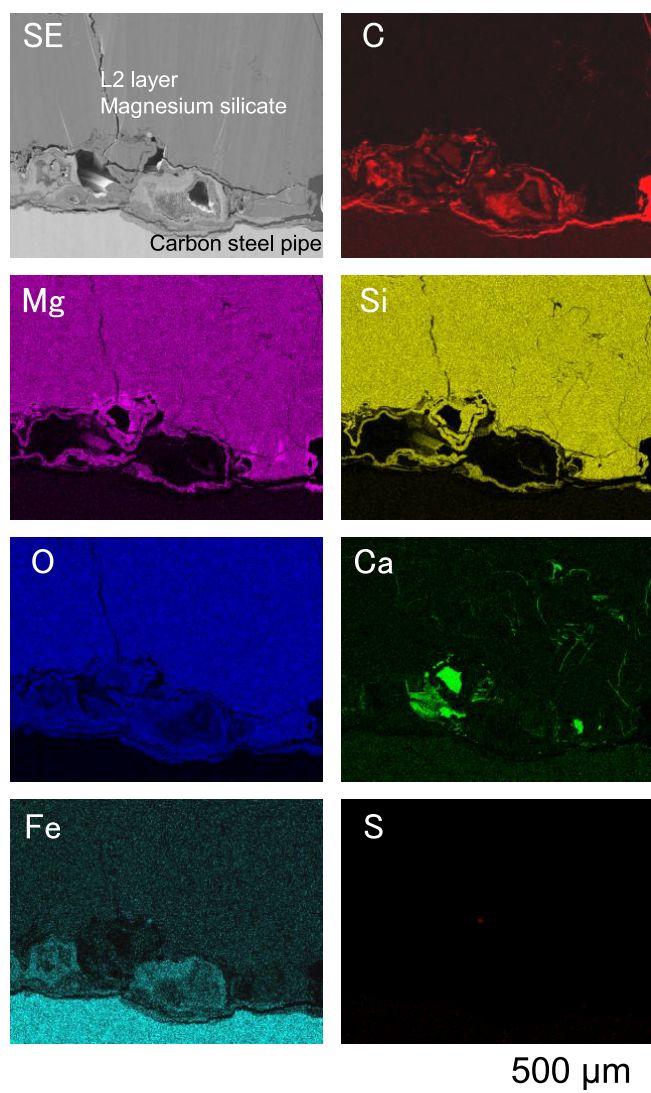


Fig. 12 Secondary electron (SE) image and element maps near the pipe surface in the longitudinal section in Fig. 3.

activation energy Q for temperatures ranging between 1,473 and 1,673 K have been previously reported to be $7.15 \times 10^{-3} \text{ m}^2/\text{s}$ and 416 kJ/mol, respectively¹⁴). However, no diffusion coefficient has been reported at lower temperatures; therefore, we used the effective diffusion coefficient of Ca at 323 K in bentonite (which consists primarily of silicate minerals), $D = 3.30 \times 10^{-11} \text{ m}^2/\text{s}$ ^{15–17}, and approximated the diffusion distance of Ca in silicate over one month as 9.25 mm. The thickness of the magnesium silicate layer in contact with hot water is 1 mm at most, which is a condition in which calcium is sufficiently supplied to the magnesium silicate layer. The above examination satisfies all these assumptions.

4.4 Modeling the scale formation process

Figure 13 is a schematic of the scale formation process on the inner wall of carbon steel pipes during the flow of geothermal hot water; the schematic was prepared based on the analytical results of this study. When the geothermal hot water starts to flow within the carbon steel pipe, corrosion first begins on the inner wall of the pipe (Fig. 13(a)–(b)). Subsequently, Fe^{2+} is dissolved into the geothermal hot water,

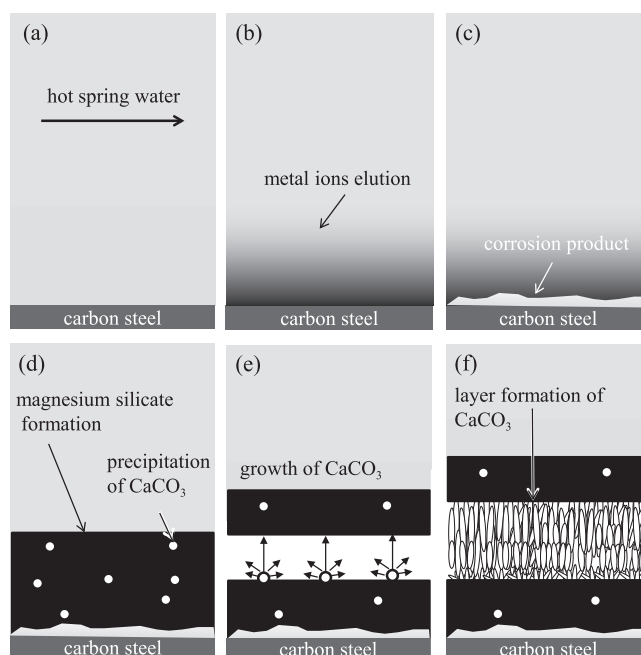


Fig. 13 Schematic illustration of a scale formation model for transporting hot spring water.

forming corrosion products (Fig. 13(c)). This process is followed by corrosion products providing heterogeneous nucleation sites for the formation of magnesium silicate, and this forms the magnesium silicate layer covering the corrosion product (Fig. 13(d)). At the same time, in the magnesium silicate layer, Ca, C, and O diffused from the geothermal hot water start to form a solid solution, and calcium carbonate (aragonite) nucleates (Fig. 13(d)–(e)). Aragonite crystals then grow along the heat flux direction (Fig. 13(e)–(f)). In this paper, we develop a conceptual model, but a kinetic analysis of precipitation conditions and growth rate based on this model is necessary in the future.

While the formation of the magnesium silicate layer (the first-stage scale) takes place over one month, the subsequent calcium carbonate layer shows rapid growth in less than a month (Fig. 10(c)). To suppress scaling of the inner walls of the pipe, surface treatments (modifications) are currently being examined, including doping with elements that can suppress adhesion of magnesium silicate and/or diffusion of Ca, C, and O from the geothermal hot water to magnesium silicate¹⁸).

5. Conclusions

Hot spring water (prior to aeration tank) was made to flow through an elbow pipe installed at the Obama hot spring binary power plant at Obama town, Unzen city, Nagasaki, and the adhered scales within the pipe were analyzed. The following conclusions were drawn based on the basic structure of the adhered scales and their formation process, and a conceptual model of scale formation process was presented.

- (1) The scales within the pipe have a four-layered structure (carbon steel pipe/iron corrosion product/magnesium silicate/aragonite/magnesium silicate). Magnesium silicate and aragonite were supersaturated in geothermal hot

water.

- (2) The surface of the carbon steel was corroded, and corrosion products were adhered to the pipe along its entire surface. In addition, the initial scale derived from the geothermal hot water was determined to be magnesium silicate, which formed as if to cover the corrosion product surface.
- (3) The calcium carbonate crystalline polymorph aragonite was not observed in the area in direct contact with the geothermal hot water, and was covered by the magnesium silicate layer. Ca, C, and O, present in a solid solution state within the magnesium silicate layer, formed calcium carbonate in mass or layer structures. By nucleating and growing crystals within the magnesium silicate layer, aragonite forms a layer that splits the magnesium silicate layer into two layers. The aragonite also had a columnar structure, and the direction of crystal growth was affected by heat flux direction.

Acknowledgements

These findings were the results of a project commissioned by the New Energy and Industrial Technology Development Organization (NEDO). The field study was performed with the cooperation of EDIT Co., Ltd., Hotel Orange Bay, and Obama Onsen Energy. In addition, Assistant Professor Eiji Yamasue of the Graduate School of Energy Science, Kyoto University, provided us with valuable discussions on diffusion phenomena. We would like to express our sincere gratitude to them.

REFERENCES

- 1) J. MacAdam and S.A. Parsons: *Rev. in Env. Sci. and BioTec.* **3** (2004) 159–169.
- 2) J. MacAdam and S.A. Parsons: *Water Sci. Technol.* **49** (2004) 153–159.
- 3) J.D. Doyle, K. Oldring, J. Churchley and S.A. Parsons: *Water Res.* **36** (2002) 3971–3978.
- 4) K. Sawada, G. Kannno, M. Iino and K. Sato: *Zairyo-to-Kankyo* **60** (2011) 296–303.
- 5) L.N. Plummer and E. Busenberg: *Geo. et Cosmo. Acta* **46** (1982) 1011–1040.
- 6) M. Hosoi and H. Imai: *J. Geothermal Research Soc. Japan* **4** (1982) 127–142.
- 7) T. Hauksson and S. Porhallsson, E. Gunnlaugsson and A. Albertsson: *Proceedings of the World Geothermal Congress, (International Geothermal Association 1995)*, 2487–2490.
- 8) I. Gunnarsson, S. Arnórsson and S. Jakobsson Science Institute Report RH-06-02, University of Iceland, 1-67.
- 9) K. D. Demadis: *The science and technology of industrial water treatment*, (CRC press, London, New York, 2010) pp.179–203.
- 10) K.D. Demadis: *Chem Process* **66** (2003) 29–32.
- 11) T. Yokohama and T. Tarutani: *J. Hot Spring Sci.* **30** (1979) 75–83.
- 12) S. Hayakawa, K. Tsuru, C. Ohtsuki and A. Osaka: *J. Am. Ceram. Soc.* **82** (1999) 2155–2160.
- 13) H. Esaka, K. Fujita, H. Daimon, M. Tamura and K. Shimozuka: *J. Japan Inst. Met. Mater.* **64** (2000) 1206–1211.
- 14) M. Morioka: *Geochim. Comochi, Acta* **45** (1981) 1573–1580.
- 15) Y. Tochigi, Y. Tachi: *JAEA-Data/Code 2008-035*(2009).
- 16) Y. Tochigi, Y. Tachi: *JAEA-Data/Code 2009-029*(2009).
- 17) Y. Tachi, Y. Tochigi, T. Suyama, Y. Saito, M. Ochs and M. Yui: *JAEA-Data/Code 2009-029*(2009).
- 18) M. Morita, R. Hashimoto, K. Sato, and M. Shirai: *JP Patent*, P2015-176398A.